ChemComm

Accepted Manuscript

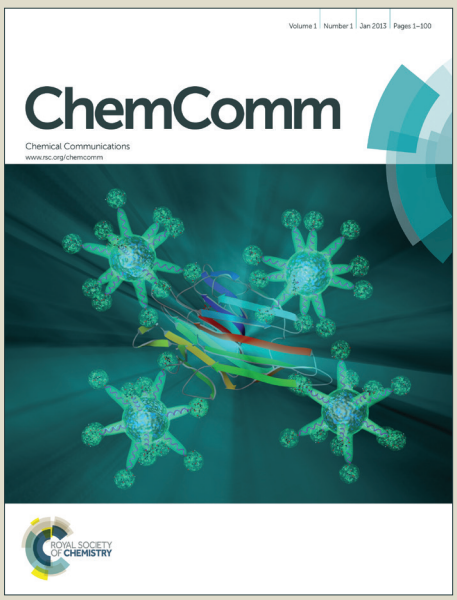

ROYAL SOCIETY OF CHEMISTRY

www.rsc.org/chemcomm

Journal Name

COMMUNICATION

Self-Sacrificial Template-Induced Modulation of Conjugated Microporous Polymer Microcapsules and Shape-Dependent Enhanced Photothermal Efficiency for Ablation of Cancer Cells

Received 00th January 20xx,
Accepted 00th January 20xx

DOI: 10.1039/x0xx00000x

www.rsc.org/

Jing Tan,[a] Jiaxun Wan,[a] Jia Guo*[a] and Changchun Wang[a]

One-step synthesis of nanosale conjugated microporous polymer (NCMP) capsules is presented by using PMAA microspheres as self-sacrificial templates. Precise control over the morphology, nanostructure and shell thickness makes the NCMPs have tunable NIR absorption ability and shape-dependent photothermal conversion efficiency. Upon exposure to 808 nm light, they rapidly generate heat (100 μg/mL) and cause thermal ablation of Hela cells and less than 10% viability.

Conjugated microporous polymers (CMPs), which are composed of conjugated organic skeletons into a microporous network, have aroused much attention for multiple applications.[1] Since the advent of the first CMP,[2] synthetic tricks for designing CMPs have been explored to modulate the compositions, topological structures and porosity for enhancing their functionalities. Compared with the early reported CMP solids synthesized without control, nanoscale CMPs (NCMPs) with the solution-dispersible characteristic are more readily tailored in morphology, size and surface chemistry, and they have been developed into versatile forms including solid microspheres,[3] hollow capsules[4] and nanotubes.[5] In our group, we investigated the confined growth of CMP networks in the miniemulsion system.[3] Not only the organic functional units (e.g. metalloporphyrin, tetraphenylene ethylene),[6] but inorganic nanoparticles (e.g. Fe_3O_4, Pd) have either been covalently bonded to organic skeletons or incorporated within porous frameworks.[7] This route seems flexible and effective to expand NCMP variety, but some issues are hard to be circumvented, for example, poor solubility of polar monomers and catalysts in aploar oil-phase droplets, inferior stability of miniemulsion under harsh reaction conditions, and hard removal of residual surfactants from the CMP particles. Without any additives, Son and co-workers adopted the template-mediated (e.g. SO_2, MOF and Fe_3O_4) precipitation polymerization to construct a core/shell microsphere and then eliminate template to give a hollow-inside NCMP with the freely standing CMP shell.[4,8] Although this method needs to pay more attention on control of CMP formation, the obtained products could possess adjustable colloidal architectures and collective properties for the broader applications. As we know, this template-mediated strategy has been widely applied to fabricate a variety of porous capsules with the shells consisting of carbon, silica or polymers.[9]

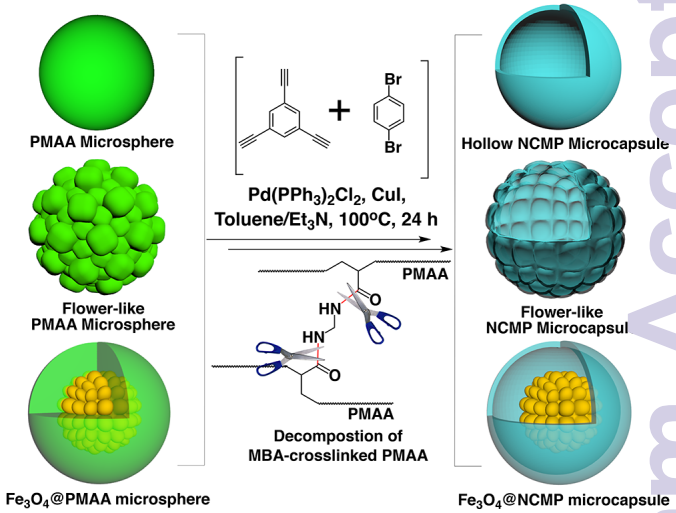

Scheme 1. Illustration of the modulation of NCMP nanostructures by using the various PMAA microspheres as self-sacrificial templates.

Near-infrared (NIR) photothermal therapy using nanoparticles have gained much interest as a minimally invasive and efficient treatment for cancer.[10] The commonly used photothermal agents are gold-based nanoparticles,[11] whereas they have been questioned for potential shape-dependent toxicity in vivo,[12] albeit with showing prominent cytocompatibility. Recently, there has been a shift towards using carbon-based nanomaterials and conjugated polymers due to their potentially better biocompatibility and high photothermal conversion efficiency.[13] To our knowledge, there is no reports concerning the potential of CMPs in bio-applications. We envision access to design NCMPs as photothermal agents due to their highly crosslinking conjugated networks, which lead to the decrease of the energy gap and the red-shift of the main absorption

[a] State Key Laboratory of Molecular Engineering of Polymers, Collaborative Innovation Center of Polymers and Polymer Composite Materials, Department of Macromolecular Science, and Laboratory of Advanced Materials, Fudan University, Shanghai 200433, P.R. China.
* E-mail: guojia@fudan.edu.cn

Electronic Supplementary Information (ESI) available: Materials and Methods, Figs. S1-S10. See DOI: 10.1039/x0xx00000x

peak to the longer-wavelength region. Also, the high surface areas with opening pore channels allow for the rapid diffusion of generated heat from the conjugated skeletons to the surroundings.[14] Herein, one-step strategy is proposed to construct the NCMP microcapsules with desired morphologies and functions. As illustrated in Scheme 1, three kinds of the crosslinked poly(methacrylic acid) (PMAA) microspheres are applied as templates to anchor the metal-based catalysts with abundant carboxylate groups on PMAA chains. 1,4-Dibromobenzene and 1,3,5-triethynylbenzene are polymerized by using the Pd(II)/Cu(I)-catalyzed Sonogashira coupling reaction to achieve a microporous poly(aryleneethynylene) shell. Accompanied by progressive formation of CMP shell, amide bonds of *N,N'*-methylene bisacrylamide (MBA), the crosslinker of PMAA particles, could be cleaved and the unlocked PMAA chains are dissolved to leave a hollow cavity and a freely standing CMP nanoshell in one step.

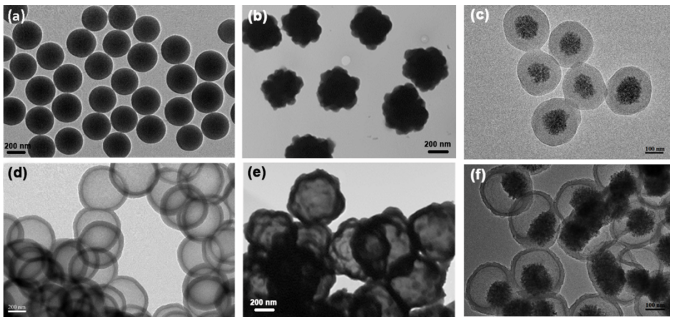

Figure 1. TEM images of (a) PMAA microspheres, (b) flowerlike PMAA microspheres, (c) Fe_3O_4@PMAA, (d) H-NCMP, (e) F-NCMP, and (f) Fe_3O_4@H-NCMP.

TEM images in Figures 1a-1c display the template particles with different morphologies and structures. The low crosslinked PMAA microspheres are uniform both in size and morphology (Figure 1a); as the crosslinking density increased from 20% to 50%, the particle surface becomes rough and the overall morphology is flower-like with slight increase in size (Figure 1b). By virtue of the reflux precipitation polymerization, PMAA could well encapsulate the Fe_3O_4 nanoclusters to give a defined core/shell nanostructure (Figure 1c). The three template particles were then applied to modulate the NCMP nanostructures. As shown in Figures 1d, when the monodispersed PMAA microspheres were used as template, the corresponding products appear a hollow cavity and a regular shell with a uniform thickness of 40 nm. Also, the flower-like NCMP (F-NCMP) and the magnetic NCMP (Fe_3O_4@H-NCMP) are obtained (Figures 1e and 1f), respectively, once the designed PMAA templates were applied. As control, the bulk CMPs synthesized without using PMAA templates exhibit a nanotube morphology (Figure S1a in ESI), indicating that the formation of NCMP capsules is mediated by the self-sacrificial PMAA microspheres. By varying the reaction conditions including solvent species, reaction temperatures and PMAA crosslinkers, we found that if triethylamine is used as co-catalyst and solvent, the amide bonds of crosslinker MBA would be broken, and the PMAA chains are unlocked and spread out across the shell. TGA results imply that there are no PMAA chains remaining within the formed microcapsules (Figure S2 in ESI). To further prove the assumption, divinylbenzene (DVB) was used to crosslink PMAA particles, and they were subjected to the same template-mediated polymerization. As observed, the hollow cavity didn't form, revealing that there is no PMAA template decomposing in the reaction (Figure S3 in ESI). Additionally, we found that the elevated temperature is helpful to elimination of PMAA template for a complete hollow inside (Figure S4 in ESI).

To tune the shell thickness, we varied the feeding amount of PMAA particles from 240 to 80 mg under otherwise identical conditions. As displayed in Figure 2, the thickness of CMP shell increases from 30, 50, 100 to 140 nm. Interestingly, the overall sizes of samples keep invariant around 500 nm. With increase in shell thickness, the diameters of the hollow cavity accordingly decrease. We suppose that because Pd/Cu catalysts could be captured by the numerous carboxylate groups of PMAA, CMP is thus locally formed on the periphery of template particles by the catalysis of immobilized metals. As the relative concentrations of monomers increase, in-situ polymerization would further progress from outside to inside, and therefore, the formed shell is thicker and the inner space is reduced. This is an interesting phenomenon result from soft-template-mediated in-situ polymerization, differing with the early reported.[4] Additionally, the overall particle size could be reduced to less than 200 nm by using the smaller PMAA microspheres, which provides a possibility for their potential use in vivo (Figure S5 in ESI).

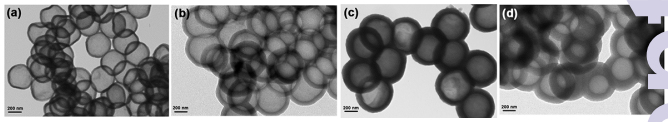

Figure 2. TEM images of a series of hollow NCMPs with different shell thickness and hollow cavity size.

Table 1. Porosity parameters of various NCMP microcapsules.

	S_{BET} (m^2/g)[a]	S_{micro} (m^2/g)[b]	V_{micro} (cm^3/g)[b]	V_{tot} (cm^3/g)[c]
H-NCMP-40	477	311	0.12	0.16
H-NCMP-100	554	373	0.15	0.19
F-NCMP-100	598	443	0.18	0.20
Fe_3O_4@H-NCMP-100	383	304	0.12	0.14

[a]Surface area is calculated from the N_2 adsorption isotherm using the Brunauer–Emmett–Teller (BET) method. [b]The micropore surface areas and pore volumes are obtained using the t-plot method based on the Halsey thickness equation. [c]Total pore volume at $P/P_0 = 0.99$.

Because the PMAA-mediated method could modulate the shell thickness, morphology and nanostructure, their effect on microporosity was then studied. Through measurement of the N_2 isotherm sorption at 77K, the results, which include surface area and pore volume, were compiled in Table 1. As the shell thickness of H-NCMP increases from 40 to 100 nm, the corresponding surface area is enhanced from 477 to 554 m^2/g. When the shell thickness was kept at 100 nm, F-NCMP gives the maximum S_{BET} up to 59[illegible] m^2/g. Compared with the hollow microcapsules, the rattle-type Fe_3O_4@NCMP have the reduced surface area and pore volume, owing to the presence of Fe_3O_4 nanocluster with no contribution for microporosity. All of the N_2 adsorption-desorption isotherms have almost the same shape (Figure S6 in ESI), showing typical type I

sorption. In accordance to the IUPAC classification, they are of microporous character. Thus, the dominant surface areas and pore volumes are derived from micropores, and their changing trend is almost synchronized with the total surface areas and pore volumes. Pore size distribution was calculated by the nonlocal density functional theory (NLDFT) model, and all of the samples show the main distributions in micropore size region (Figure S7 in ESI). This is a plausible population as a result of micropore character.

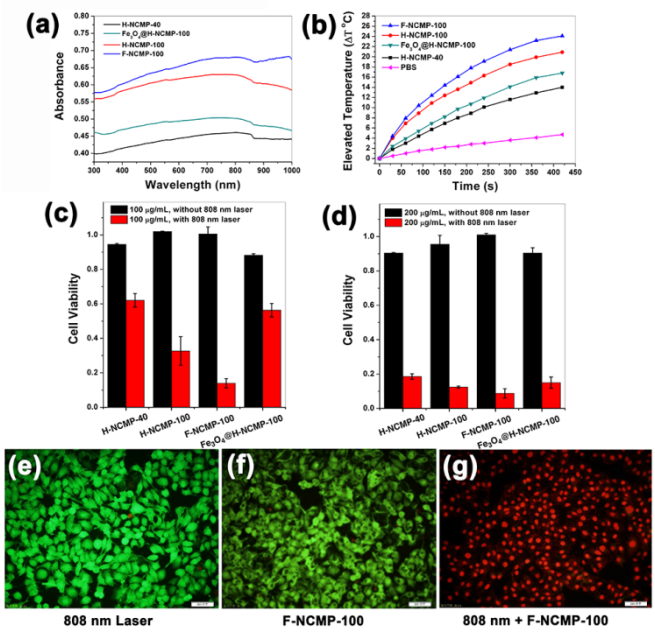

Figure 3. (a) UV-vis-NIR spectra of NCMPs in PBS at a concentration of 100 μg/mL; (b) Elevated Temperature change for NCMPs (200 μg/mL) and PBS under 808-nm laser irradiation for 6 min (5 W/cm^2); Cell viability of Hela cells with (c) 100 and (d) 200 μg/mL of NCMPs exposed to 808-nm laser (5 W/cm^2) for 5 min; Fluorescence images of Hela cells treated by (e) Laser (808 nm, 5 W/cm^2, 5 min); (f) F-NCMP-100 (200 μg/mL); (g) Laser (808 nm, 5 W/cm^2, 5 min)+ F-NCMP-100 (200 μg/mL). Live and dead cells stained by calcein AM and propidium iodide dyes show green and red colors, respectively.

To investigate the photothermal conversion effect, the UV-*vis*-NIR spectra of a series of samples were recorded as seen in Figure 3a. The broad absorption covering visible and NIR windows were observed for all of the samples at the same concentration of 100 μg/mL in phosphate buffered saline (PBS), implying that a large conjugated network within CMP nanoshell gives rise to the decrease of energy gap and the red-shift of absorption towards long wavelengths, as similar as carbon nanotube[15] and graphene.[16] The maximum absorption is found at ~800 nm, and the absorption ability of F-NCMP-100 is the stronger than the others. To verify their potential in photothermal conversion, the sample dispersions in PBS were exposed to an 808 nm NIR laser at a power density of 5 W/cm^2 within a short time (Figure 3b). PBS aqueous solution just shows a little temperature change. In contrast, the dispersions of NCMPs enabled a burst increase of temperature upon irradiation of 808-nm laser for 6 min, and the greatest heating was generated on F-NCMP-100, giving a rising temperature of 24 ^{o}C in 6 min. Also, the enhanced shell thickness of H-NCMP is able to improve the photothermal conversion, proving the crucial role of CMP nanoshell (Figure S8 in ESI). As compared to the F-NCMP-100 with the same shell thickness, it is very interesting that the rough surface allows for generating more heat. We suppose that the oscillating electric field of a light wave acts on the charges to mediate the formation of radiating dipoles within particles for light scattering. The F-NCMP surface containing many discrete "islands" with the small domain of less than 100 nm may enhance the scattering effectiveness and increase the average optical path in medium, thereby facilitating NIR light absorption for a large photothermal conversion. Prior to determine the efficiency of killing cancer cells, in-vitro cytotoxicity assays were performed in the absence of NIR laser. As shown in Figures 3c and 3d, all of the NCMPs have no significant cytotoxic effect to Hela cells as well as 293T cells (Figure S9 in ESI). Also, the estimated hemolysis rates were lower than 5% for various concentrations of NCMPs, indicative of their blood compatibility (Figures S10 in ESI). Cell ablation studies were performed by irradiating the cell solutions with an 808 nm laser for 5 min (5 W/cm^2) in the presence of samples. For the two H-NCMPs at concentration of 100 μg/mL, the 100-nm CMP shell is responsive for more pronounced ablation of Hela cells, giving less than 40% of cell viability, whereas the F-NCMP could give 10% of cell viability under identical conditions. This proves again the shape-dependent enhanced photothermal conversion efficiency. When the concentrations increased to 200 μg/mL, cell viability was declined to less than 10%. Furthermore, due to the rapid magnetic responsiveness of Fe_3O_4@H-NCMP, they could achieve target delivery with applied magnetic field. Besides, we observed the cell states by using fluorescence microscope. As seen in Figures 3e-3g, the thermal ablation of Hela cells is effective only upon exposure to NIR with F-NCMP as photothermal agent.

In summary, we propose the one-step approach to preparing hollow NCMP microcapsules using PMAA as self-sacrificial template and modulate the morphology and nanostructure of template particles to achieve the flower-like and rattle-type NCMP microcapsules. Also, with increase of the thickness of CMP nanoshell by varying monomer concentrations, the absorption capability in visible and NIR regions is improved and shows a shell-dependent enhancing tendency. When NIR irradiation (808 nm, 5 W/cm^2) is applied to a series of NCMPs in PBS solution, F-NCMP (100 μg/mL) generates the greatest heat with changing the temperature by 24 ^{o}C in 6 min. Also, cell viability assays show that F-NCMP outperforms other NCMPs in generating heat to destroy Hela cells in vitro upon irradiation by NIR light. This study confirms a new attractive potential of nanoscale CMP for medical application and also, because of the possibility for drug loading in pores, they will be useful in multimodal treatment where chemotherapy and hyperthermia are both acquired.

We acknowledge the financial support of the NSFC (21474015) and STCSM (13520720200 and 14ZR1402300).

References

1 Y. H. Xu, S. B. Jin, Hong Xu, A. Nagai and D. L. Jiang, *Chem. Soc. Rev.*, 2013, **42**, 8012; K. Y. Wu and J. Guo, *Acta Chim. Sinica*, 2015, **73**, 480.
2 J.-X. Jiang, F. B. Su, A. Trewin, C. D. Wood, N. L. Campbell, H. J. Niu, C. Dickinson, A. Y. Ganin, M. J. Rosseinsky, Y. Z. Khimyak and A. I. Cooper, *Angew. Chem. Int. Ed.*, 2007, **46** 8574.

3 P. Zhang, Z. H. Weng, J. Guo and C. C. Wang, *Chem. Mater.*, 2011, **23**, 5243.
4 N. Kang, J. H. Park, M. Jin, N. Park, S. M. Lee, H. J. Kim, J. M. Kim and S. U. Son, *J. Am. Chem. Soc.*, 2013, **135**, 19115.
5 N. Kang, J. H. Park, J. Choi, J. Jin, J. Chun, I. G. Jung, J. Jeong, J.-G. Park, S. M. Lee, H. J. Kim and S. U. Son, *Angew. Chem. Int. Ed.*, 2012, **51**, 6626.
6 K. Y. Wu, J. Guo and C. C. Wang, *Chem. Commun.*, 2014, **50**, 695; P. Zhang, K. Y. Wu, J. Guo and C. C. Wang, *ACS Macro Lett.*, 2014, **3**, 1139.
7 P. Zhang, J. Guo and C. C. Wang, *J. Mater. Chem.*, 2012, **22**, 21426; L. Y. You, Y. T. Zhang, S. Xu, J. Guo and C. C. Wang, *ACS Appl. Mater. Interfaces*, 2014, **6**, 15179; S. Xu, Z. H. Weng, J. Tan, J. Guo and C. C. Wang, *Polym. Chem.*, 2015, **6**, 2892.
8 J. Chun, S. Kang, N. Park, E J. Park, X. Jin, K.-D. Kim, H. O. Seo, S. M. Lee, H. J. Kim, W. H. Kwon, Y.-K. Park, J. M. Kim, Y. D. Kim and S. U. Son, *J. Am. Chem. Soc.*, 2014, **136**, 6786; J. Yoo, N. Park, J. H. Park, J. H. Park, S. Kang, S. M. Lee, H. J. Kim, H. Jo, J.-G. Park and S. U. Son, *ACS Catal.*, 2015, **5**, 350.
9 Y. Chen, P. Xu, M. Wu, Q. Meng, H. Chen, Z. Shu ,J. Wang , L. Zhang , Y. Li and J. L. Shi, *Adv. Mater.*, 2014, **26**, 4294; G. A. Ferrero, A. B. Fuertes and M. Sevilla, *J. Mater. Chem. A*, 2015, **3**, 2914; J. Hu, X. Wang, L. Liu and L. Wu, *J. Mater. Chem. A*, 2014, **2**, 19771; Z. Teng, X. Su, Y. Zheng, J. Zhang, Y. Liu, S. Wang, J. Wu, G. Chen, J. Wang, D. Y. Zhao and G. M. Lu, *J. Am. Chem. Soc.*, 2015, **137**, 7935; B. Li, X. Yang, L. Xia, M. I. Majeed and B. Tan, *Sci. Rep.*, 2013, **3**, 2128
10 A. M. Gobin, M. H. Lee, N. J. Halas, W. D. James, R. A. Drezek and J. L. West, *Nano Lett.*, 2007, **7**, 1929.
11 Z. J. Zhang, J. Wang, X. Nie, T. Wen, Y. L. Ji, X. C. Wu, Y. L. Zhao and C. Y. Chen, *J. Am. Chem. Soc.*, 2014, **136**, 7317; Z. J. Zhang, L. M. Wang, J. Wang, X. M. Jiang, X. H. Li, Z. J. Hu, Y. L. Ji, X. C. Wu and C. Y. Chen, *Adv. Mater.*, 2012, **24**, 1418.
12 S. Sharifi, S. Behzadi, S. Laurent, M. L. Forrest, P. Stroevee and M. Mahmoudi, *Chem. Soc. Rev.*, 2012, **41**, 2323; N. Lewinski, V. Colvin and R. Drezek, *Small*, 2008, **4**, 26.
13 L. G. Xu, L. Cheng, C. Wang, R. Peng, Z. Liu, *Polym. Chem.*, 2014, **5**, 1573; L. Cheng, C. Wang, L. Z. Feng, K. Yang and Z. Liu, *Chem. Rev.*, 2014, **114**, 10869.
14 J. Tian, T. Kim, T. J. Lu, H. P. Hodson, D. T. Queheillalt, D. J. Sypeck and H. N. G. Wadley, *Int. J. Heat Mass Transfer*, 2004, **47**, 3171.
15 H.-K. Moon, S.-H. Lee and H.-C. Choi, *ACS Nano.*, 2009, **3**, 3707.
16 K. Yang, S. Zhang, G. X. Zhang, X. M. Sun, S.-T. Lee and Z. Liu, *Nano Lett.*, 2010, **10**, 3318; J. T. Robinson, S. M. Tabakman, Y. Liang, H. Wang, H. Sanchez Casalongue, D. Vinh and H. Dai, *J. Am. Chem. Soc.*, 2011, **133**, 6825.